Materials and Design 157 (2018) 97–104

Contents lists available at ScienceDirect

Materials and Design

journal homepage: www.elsevier.com/locate/matdes

Strength enhancement and density reduction by the addition of Al in CrFeMoV based high-entropy alloy fabricated through powder metallurgy

Ahmad Raza [a], Ho Jin Ryu [b,*], Soon Hyung Hong [a,*]

[a] Department of Materials Science and Engineering, Korea Advanced Institute of Science and Technology (KAIST), 291 Daehak-ro, Yuseong-gu, Daejeon 34141, Republic of Korea
[b] Department of Nuclear and Quantum Engineering, Korea Advanced Institute of Science and Technology (KAIST), 291 Daehak-ro, Yuseong-gu, Daejeon 34141, Republic of Korea

HIGHLIGHTS

- The Al addition promoted the BCC2 phase formation in the primarily single-phase CrFeMoV alloy.
- The content of BCC2 varied directly with the concentration of Al.
- The Al introduction decreased the density and improved the yield strength and hardness.
- The Al_xCrFeMoV systems showed highest specific yield strength as compared to previously reported high entropy alloys.

GRAPHICAL ABSTRACT

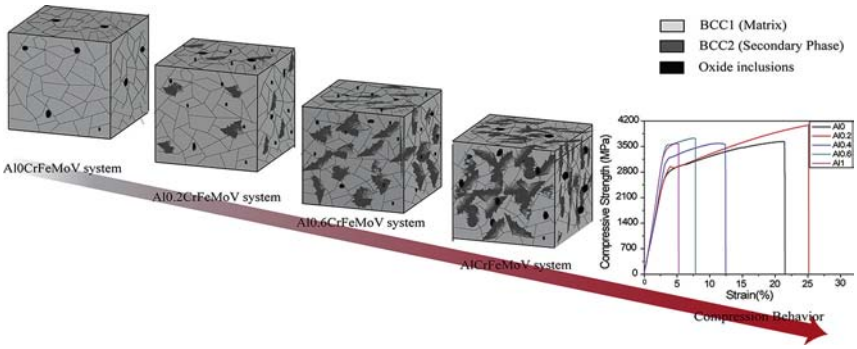

ARTICLE INFO

Article history:
Received 28 March 2018
Received in revised form 7 July 2018
Accepted 9 July 2018
Available online 21 July 2018

Keywords:
High entropy alloy
Thermodynamic parameters
Powder metallurgy
Microstructure analysis
Mechanical characteristics

ABSTRACT

The influence of Al addition to the microstructure and specific mechanical properties of CrFeMoV-based quaternary high-entropy alloy (HEA) is investigated in this study. The designed Al_xCrFeMoV alloys were fabricated through a powder metallurgy process using high-energy planetary ball milling followed by spark plasma sintering (SPS). Methanol (2.5 wt%) was used as a process aid during the mechanical alloying. Comprehensive microstructural examination revealed that the addition of Al led to the appearance of a BCC2 phase whose volume was directly related to the Al concentration. The experimental results were in good agreement with an inclusive thermodynamic analysis and predictions. The appearance of the BCC2 phase, and the strong bonding energy of Al and solid-solution strengthening in Al-containing systems, significantly enhanced the yield strength in compression from 2730 to 3552 MPa in the Al_xCrFeMoV (x = 0 to 0.6) system at ambient temperature. The most notable feature of this study is the compressive strength that increased with decreasing density. The Al-1 (Al_x where x = 1) alloy displayed a specific yield strength and hardness that are greater than those for any previously reported HEA, approaching 512 MPa·cm^3/g and 140 HV·cm^3/g, respectively.

1. Introduction

Contemporary materials research is extending the boundaries of processing technologies. Metals and alloys are essential aspects of engineering technology. The development of new fabrication techniques and alloy designs to realize improved material characteristics is

* Corresponding authors.
E-mail addresses: hojinryu@kaist.ac.kr (H.J. Ryu), shhong@kaist.ac.kr (S.H. Hong).

https://doi.org/10.1016/j.matdes.2018.07.023
0264-1275/

necessary to keep up with rapid advancements in technologies [1,2]. Conventional alloy design, which is based on a single element as the major contributor with several other minor alloying elements, is reaching its limits in terms of properties for applications requiring low density, high yield strength, high corrosion resistance and high creep resistance [2,3]. Especially, the aerospace, automobiles, and other transportation industries are looking forward to new dimensions in the alloys with lower density and higher strength to reduce the weight and fuel consumption. A new concept in alloy design, called high-entropy alloy (HEA), has evolved in modern metallurgy. It is based on the contribution of five or more alloying elements whose contents range from 5 to 35 at.% [4,5]. To exceed these limitations, several researchers have designed quaternary alloys, as well as alloys with numerous contributing elements having weight fractions lower or higher than the nominal ranges [6,7]. These evolved alloys are called multi-principal element alloys [8–10]. Choosing the elements to realize required alloy properties is a very important process in the design of HEAs [10]. Thermodynamic constraints used to predict phase formation in these unusual high-entropy, heavily disordered alloys [11] are based on atomic size difference (δ) [12–15], valence electron concentration (VEC) [16–18], the ratio Φ of configurational entropy of mixing (S_c) to excessive entropy of mixing (S_E) [19–21], the enthalpy of mixing (ΔH) [14,17], and the ratios of ΔH and ΔS_{conf} to the Gibbs free energy (Ω) [13,21]. Such predictions confine the number of systems meeting the required specifications of low cost and manufacturability [8]. This approach has enabled the development of numerous HEA systems displaying extraordinary mechanical properties.

HEAs can be divided into two types according to their elemental compositions, i.e., (1) those based on Ni, Co, Fe, Mn, Cu and Cr, and (2) those using Cr, V, Mo, Ta, W, Hf, Nb, Zr and Ti as the main elements [22]. HEAs in the first category mostly form face-centered cubic (FCC) structures or a combination of FCC and body-centered cubic (BCC) structures; the second category of HEAs mostly forms BCC structures [23–28]. Cantor alloy is an outstanding example from the former category; it is based on FeCrCoNiMn and shows exceptional mechanical behavior at cryogenic temperatures [24]. However, this system has poor high-temperature characteristics [29]. In contrast, refractory HEA systems, which are often found in the latter category, have excellent high-temperature mechanical properties but insufficient ductility and toughness at room temperature [5,30].

We recently introduced a novel quaternary system, CrFeMoV, having equiatomic composition [31]. The designed composition contains elements from both of the above-described HEA categories. Although the fabricated alloy formed a single BCC phase, it had a remarkably high yield strength and reasonable ductility. Its measured density was 7.93 g/cm^3; previously reported HEAs have densities that typically range from 5.9 to 8.4 g/cm^3 [30,32]. Therefore, the density of the CrFeMoV alloy is near the upper limit. In the current study, the addition of Al_x to the CrFeMoV alloy in varying concentrations (x = 0, 0.2, 0.4, 0.6 and 1) is described. Numerous researchers have studied the effect of Al addition on the microstructure and mechanical behavior of several HEA systems [33,34]. Here, the purpose was to determine the effect of Al addition on the microstructural and mechanical behavior of HEA systems, and on density reduction. Furthermore, the thermodynamic constraints noted above predicted the appearance of an additional phase with the addition of Al; this is comprehensively discussed in microstructural and crystallographic terms. Mechanical properties were also examined via compression and microhardness testing.

2. Experimental procedure

The Al_xCrFeMoV alloys were fabricated using a powder metallurgy process, as follows. Powders of Fe, Cr, V, Mo and Al (commercial powders with a purity of 99.5%) were mixed and mechanically alloyed with varying concentrations of Al (x = 0, 0.2, 0.4, 0.6 and 1) while keeping the concentration of the rest of the elements equimolar. Mechanical alloying (MA) was performed using a high-energy planetary ball mill in tool steel jars and with WC balls, keeping the ball:powder ratio fixed at 10:1. The MA was done at 200 rpm using 2.5 wt% methanol as a process control agent (PCA) in an Ar-filled glove box. A PCA was used to avoid cold welding of the powder to the walls and balls during milling. To minimize possible contamination during alloying, the milling time was optimized, as reported previously [31]; the optimal time for all four compositions was 7 h. The milled powder was then sintered at the temperature, heating rate and pressure of 1100 °C, 100 °C/min and 50 MPa, respectively, by spark plasma sintering (SPS) (Dr. Sinter SPS-515S; Sumitomo Coal Mining Co., Ltd.).

Microstructures were examined by scanning electron microscopy (SEM) (XL30; Philips), and X-ray diffraction (XRD) (D/Max-2500; Rigaku) was used for the crystallographic characterizations. Transmission electron microscopy (TEM) (JEM2100F; JEOL Ltd.) was used to examine the crystallographic and microstructural features at the nanoscale, and elemental concentration was investigated by TEM-energy dispersive spectroscopy (TEM-EDS) (Magellan 400; FEI). Compression and microhardness testing examined the mechanical performance. The compression testing was conducted using an Instron 5982 machine with cylindrical specimens of dimensions 5 mm in height and 3 mm in diameter. For the hardness test, the Vickers microhardness was measured using a square diamond indentor (402MVD; Wolpert Wilson Instruments), with an applied load of 5 g for 10 s; and values were determined 10 times for each specimen before averaging to obtain the reported values.

3. Results

3.1. Mechanical alloying and sintering

The mechanically alloyed powder was fabricated by high-energy ball milling according to the procedure described by Raza et al. [31]. The PCA mitigated cold welding and the formation of any flakes during milling, which helped to achieve a high relative density (Fig. 1). The mechanically alloyed powder was sintered by SPS and the actual density of sintered specimen was calculated by Archimedes principle while the theoretical density was calculated by rule of mixture. The acronyms of Al-0, Al-0.2, Al-0.4, Al-0.6 and Al-1 represent each alloy; these are based on the molar fraction of Al in the Al_xCrFeMoV system.

3.2. Microstructural analysis

The morphology of the fabricated alloys was examined using SEM (Fig. 2). Each image is displayed at lower and higher magnifications to better illustrate the microstructure. The Al-0 system consists of a single-phase solid solution (SSS) with a very small volume fraction of

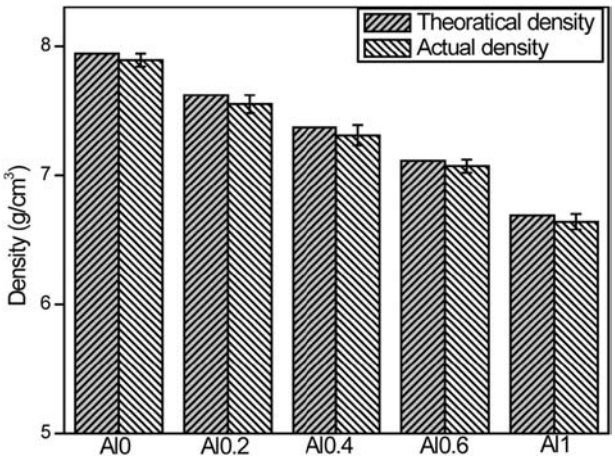

Fig. 1. Acronyms and relative densities of the Al_xCrFeMoV system.

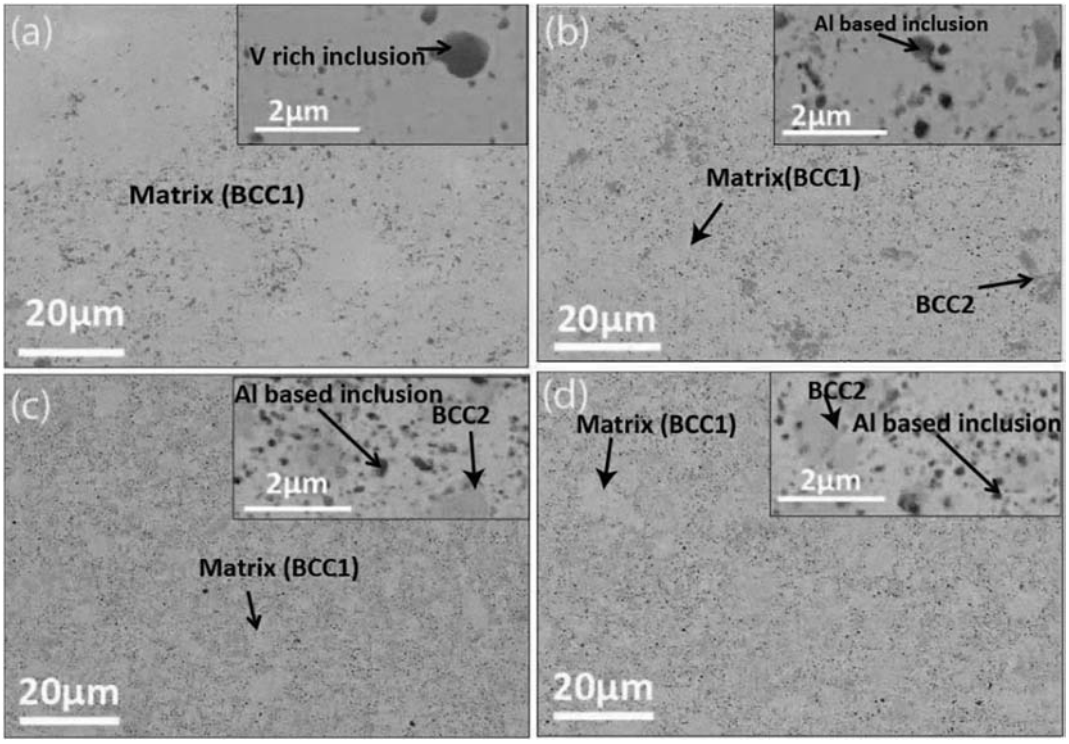

Fig. 2. Scanning electron microscopy (SEM) images of (a) Al-0, (b) Al-0.2, (c) Al-0.6 and (d) Al-1 showing the different phases.

V oxide-based inclusions (Fig. 2(a)). The addition of Al influenced the quaternary CrFeMoV system by altering the type of inclusions and triggering the appearance of a secondary phase. Aluminum is more susceptible to oxidation than V. Hence, the oxide inclusion in the Al-containing systems was Al-based (Fig. 2(b, c and d)). The oxidation likely occurred during the MA of the powder due to the very fine particle size and high surface energy. However, these fine inclusions (with diameters of 100–300 nm) helped to boost the mechanical properties of the

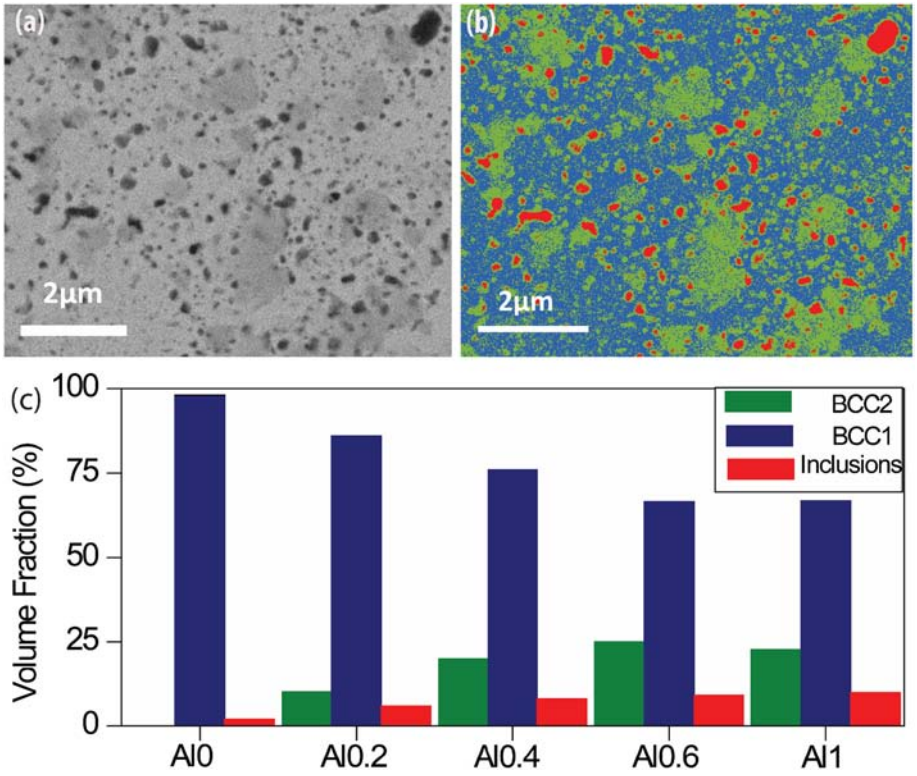

Fig. 3. Volume fraction analysis of the phases. (a) SEM image of the Al-0.6 alloy with (b) color mapping of the micrograph using MATLAB. (c) Volume fraction of the individual phases for each alloy.

fabricated alloys. The major effect on the morphology of the alloys of addition of Al was the appearance of an additional BCC phase, herein referred to as BCC2. Moreover, it is evident from comparison of the micrographs of the Al-containing alloys in Fig. 2(b, c and d) that the volume fraction of the secondary phase varied directly with the Al content. Several other studies also reported the appearance of a BCC2 phase in HEA systems with the addition of Al, instead of an intermetallic phase [2,34–38].

Image analysis (MATLAB, ImageJ) was performed to precisely measure the volume fraction of each phase (Fig. 3). Fig. 3(a) is an SEM micrograph of the Al-0.6 alloy system and Fig. 3(b) highlights each phase with a distinct color. The blue color corresponds to the matrix, while green and red correspond to the BCC2 phase and the oxide inclusions, respectively. The calculated volume fraction of all phases is shown in Fig. 3(c). The volume fraction of the oxide inclusions displayed an increment with the addition of Al. Moreover, the addition of Al caused the formation of the BCC2 phase and the volume fraction of BCC2 increased with increasing Al content, reaching 24%, 22% in the Al-0.6 and Al-1 alloy system.

The elemental composition of the various phases was assessed using EDS (Fig. 4). The points of analysis are indicated on the micrographs and the corresponding elemental composition of the respective phases are shown. The Al-0 system (Fig. 4(a)) exhibits two phases, i.e., the V-based oxide inclusions and the matrix having nearly nominal composition. The addition of Al changed the type of inclusion from V- to Al-based and caused the formation of the BCC2 phase (Fig. 4(b–d)). The BCC2 phase is enriched with V along with Cr and Mo, while Al dominates the inclusions. Moreover, the matrix phase shows the nominal concentration of all contributing elements except Al. The lower atomic percentage of Al in the BCC1 phase relative to other contributing elements may have occurred because of its consumption as oxide inclusions.

The crystal structures of the fabricated alloys were established using XRD (Fig. 5). The diffraction pattern of the Al-0 system was consistent with a single BCC phase, exhibiting peaks corresponding to the (110), (200) and (211) planes. No additional peaks for the oxide phase were apparent due to the low volume fraction of inclusions. The addition of Al led to secondary peaks of relatively low intensity in the Al-0.2, Al-0.4, Al-0.6 and Al-1 systems resulted from the dispersed oxide (Al_2O_3) inclusions; these peaks matched those for corundum. The peaks of BCC2 phase are overlapped with the peaks of BCC1 phase. The measured lattice parameters for the BCC (matrix) phase were 0.302 ± 0.001 nm.

The crystallographic features of the matrix, BCC2 phase and oxide inclusions were also examined by TEM. Fig. 6 shows TEM images and selected area electron diffraction (SAED) patterns. The image of the Al-0.6 system shows the different phases (Fig. 6(b)). The contrast is markedly superior to that of the SEM images. The grey phase corresponds to the BCC2 phase and Fig. 6(a) shows the SAED pattern of this secondary phase. The SAED pattern is centered along the [011] zone axis and represents a BCC phase with a lattice constant of 0.308 nm, which is very similar to that determined by XRD. Fig. 6(c) shows the SAED pattern of the BCC1 phase centered along the [011] zone axis; the calculated lattice parameter is 0.304 nm. There were insufficient XRD data to identify the crystallographic features of the oxide inclusions; these were very small in the Al-0.2 and the Al-0.6 systems. However, TEM images of the Al-1 system (Fig. 6(e)) show that the oxide inclusions are much larger in this alloy than in the other systems. The dark phase in the Al-1 system corresponds to inclusions. Fig. 6(d) shows the lattice fringes of the oxide inclusions with the diffraction pattern determined through fast Fourier transformation (FFT). The lattice fringes obtained from

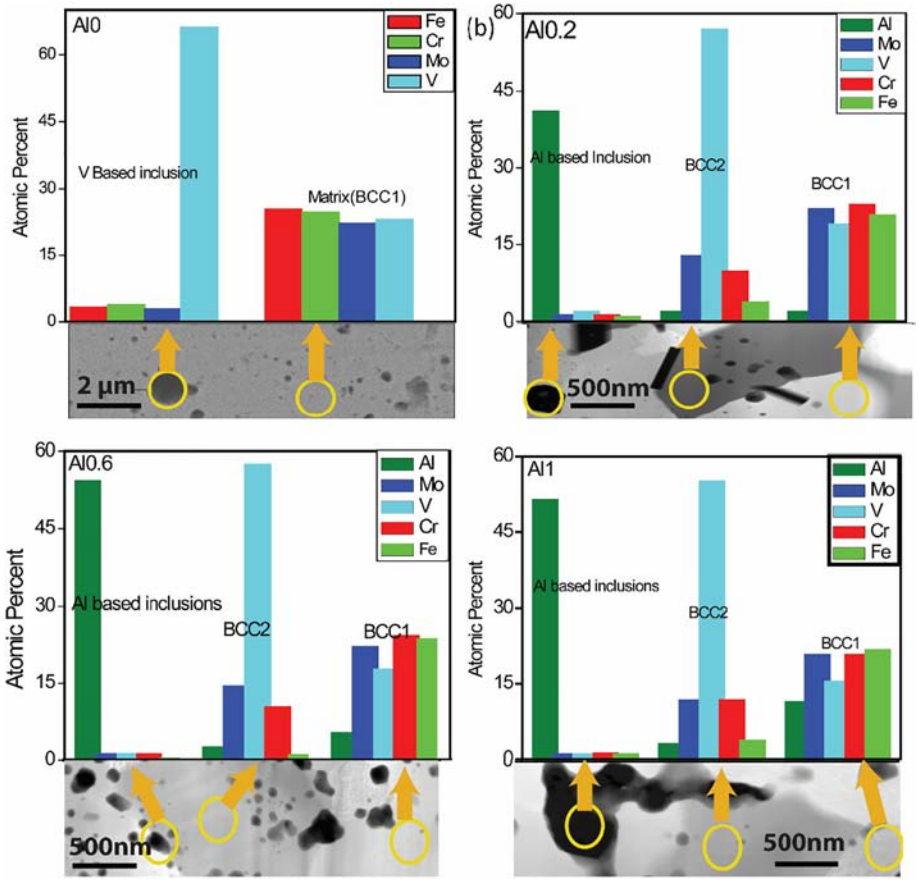

Fig. 4. Elemental analysis of phases using energy dispersive spectroscopy (EDS). (a), (b), (c) and (d) correspond to the Al-0, Al-0.2, Al-0.6 and Al-1 systems, respectively.

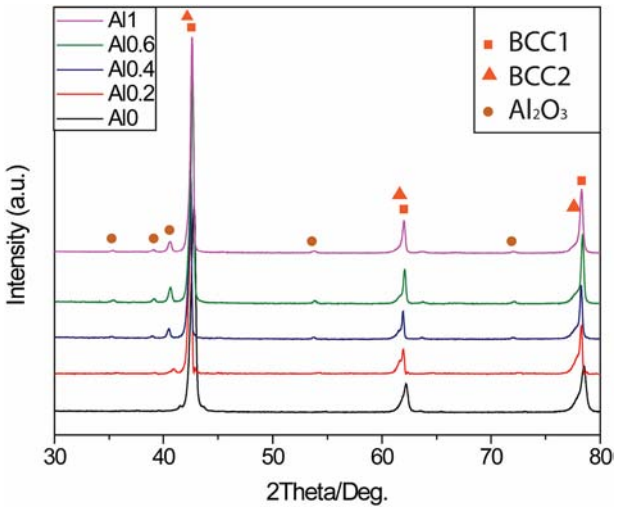

Fig. 5. X-ray diffraction (XRD) patterns.

oxide inclusions show typical ordered behavior, which is common in such compounds. The SAED pattern of the oxide inclusions is presented in Fig. 6(f); analysis of the pattern revealed the existence of a hexagonal close-packed (HCP) structure similar to that of alumina. The zone axis of the SAED pattern was [0$\bar{1}$10] and the calculated lattice parameters were a = 0.4658 nm and c = 1.287 nm. These parameters are in good agreement with reported values for α-alumina (corundum).

3.3. Thermodynamic microstructure analysis

Thermodynamic constraints play a vital role in elucidating the appearance of a BCC2 phase with the addition of Al, and the increase in volume fraction of the BCC2 phase with increasing Al content. The VEC, δ and Φ parameters are key to explaining these phenomena; their calculated values are given in Table 1. The role of each of these parameters is discussed in detail below.

The physical parameter, VEC, can predict the stability of FCC, BCC, or HCP phases for a designed system, as first described by Guo et al. [17] for HEAs. For HEAs, the VEC can be determined through the rule of mixtures, as follows:

$$\mathrm{VEC} = \sum_{i=1}^{n} c_i (VEC)_i \tag{1}$$

where c_i and VEC are the elemental concentrations and the VECs of the individual constituents of an HEA. According to Gou et al. [17], the FCC phase will be stable if the VEC ≥8, and the BCC phase will be more stable if the VEC ≤6.87. In our designed alloys, the VEC for Al-0 was 6.25, consistent with the BCC structure. Moreover, the addition of Al further decreased the VEC to 5.6 in the Al-1 alloy, which indicated that Al was playing a role as a BCC stabilizer. The experimental results are completely aligned with the predicted phase stability of the BCC phase.

Zhang et al. [39] and Yang et al. [13] demonstrated that the δ parameter can be particularly useful to evaluate the possibility of solid solution phase formation or intermetallic phase formation in a designed system. In the current systems, the value of δ was determined as follows:

$$\delta = 100 \times \sqrt{\sum_{i=1}^{N} c_i \left(1 - \frac{r_i}{\bar{r}}\right)^2} \tag{2}$$

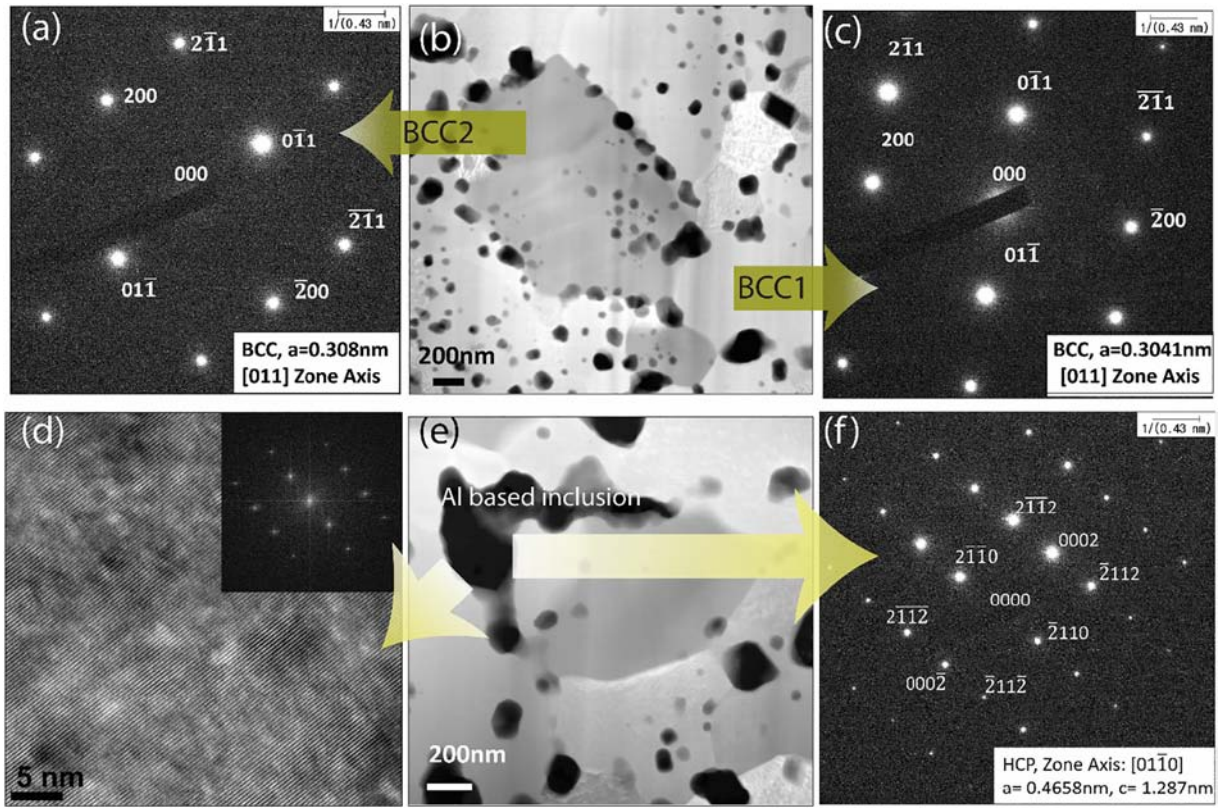

Fig. 6. Transmission electron microscopy (TEM) images and selected area electron diffraction (SAED) patterns of the (a) BCC2 and (c) BCC1 phases of the (b) Al-0.6 system, and the (d) lattice fringes of Al oxide inclusions and the (f) SAED pattern of the (e) Al-1 alloy.

Table 1
The calculated values of the thermodynamic parameters and their structure predictions.

System FeCrVMoAlx	Atomic size difference (%)	VEC	ϕ	S_c (K_b/atom)	S_E (K_b/atom)	Structure
Al-0	3.88	6.25	24.73	1.389	0.044	BCC
Al-0.2	4.18	6.09	16.55	1.435	0.057	Multiphase
Al-0.4	4.41	5.95	13.15	1.482	0.068	Multiphase
Al-0.6	4.57	5.82	10.34	1.526	0.076	Multiphase
Al-1	4.79	5.6	6.1	1.61	0.095	Multiphase

where c_i and r_i are the concentration and radius of the i^{th} element, and $\bar{r}$ is the mean radius. According to Yang et al. [13], if the value of δ lies in the range of 1–6.6%, then the system will form solid solution phases. However, if the value exceeds this limit, intermetallic phases can appear in the alloy system. Here, the δ value of the fabricated systems lay below 5% and the maximum value of 4.79% was established for the Al-1 system. This thermodynamic parameter suggests that the addition of Al to the quaternary CrFeMoV system will not lead to the formation of any intermetallic compound. However, there is a probability of an additional secondary phase forming. The results of the fabricated phases are in agreement with the δ prediction: the addition of Al resulted in the formation of an additional solid solution phase, but not an intermetallic phase.

The likelihood of the formation of a secondary phase alloy can be determined by the thermodynamic factor ϕ. This factor was introduced by Ye et al. [20,21], and can be expressed as follows:

$$\phi = -\frac{S_c - [\Delta H_{mix}]T_m}{[S_E]} \quad (3)$$

where Sc is the configurational entropy of mixing and S_E is the excess entropy of mixing that is a function of atomic size (d_i), concentration (c_i) and atomic packing factor (ξ_i) [19]. According to Ye et al. [20,21], if the value of $\phi > 20$ for a system, then the system will form an SSS. However, if the value of $\phi < 20$, then the system may be multiphasic. The $S_E(\xi_i, d_i, c_i)$ was calculated using the complex equations presented by Ye et al. [19]; our calculated values are given in Table 1. The calculated value of ϕ for the quaternary system is above 20 (24.73), and therefore predicts the formation of an SSS. However, the addition of Al decreased ϕ, which resulted from increased ΔH_{mix} (enthalpy of mixing) and $S_E(\xi_i, d_i, c_i)$. The values of ϕ for Al-0.2, Al-0.6 and Al-1 were 16.55, 10.34 and 6.1, respectively. All were <20, which predicts the formation of multiphase alloys. Interestingly, the trend of the thermodynamically calculated prediction is in good agreement with the experimentally observed microstructural and mechanical behavior of the alloys. As ϕ decreased, the volume fraction of the BCC2 phase increased and Al-1 showed the highest volume fraction of BCC2. The experimental results fully support the thermodynamic predictions; alloys having $\phi < 20$ formed multiphase structures, while Al-0 with $\phi > 20$ formed an SSS.

The V based HEAs have shown the tendency to form a V-rich solid solution phase as it also has been observed in an alloy of NbVTiZr, and NbV_2TiZr alloys [30]. In a few other studies, V based alloys form the intermetallic phases in the system [31]. In the current study, it has been observed that the trigger of formation of additional phase is Al addition, and the content of BCC2 phase increased with the addition of Al as Al-0 system showed the absence of BCC2 phase. There is no direct reference available where the addition of Al caused the formation of V-rich phase due to limited study on this issue.

3.4. Mechanical properties

Compression and nanoindentation tests were conducted to study the mechanical properties of the mechanically alloyed and sintered specimens (Fig. 7). Fig. 7(a, b) shows that the Al-0 system had exceptionally high yield strength and Vickers hardness of 2730 MPa and 667 HV, respectively, along with some ductility. The addition of 0.2 mole-fraction of Al to the Al-0 system slightly enhanced the yield strength, to 2781 MPa, and hardness to 745 HV. With further addition of Al, the yield strength of the Al-0.4 system was significantly higher at 3182 MPa and the hardness reached 851 HV. This enhancement was influenced by several factors. First, the addition of Al altered the type of oxide inclusions from V- to Al-based oxides, and the latter inclusions were smaller than the former ones. Second, Al has a higher atomic size difference relative to the other four elements in the alloy. This variation in size triggered the appearance of a secondary BCC2 phase and contributed to solid solution strengthening of the system. The uniform distribution of the BCC2 phase in the matrix also substantially improved the mechanical properties. Contributions by all these factors led to the improved strength and limited plasticity of the Al-0.4 system compared with the Al-0 and Al-0.2 systems. Moreover, the Al-0.6 system had a yield strength of 3552 MPa, with a substantial hardness of 906 HV. Although further addition of Al did not increase the strength and in fact resulted in a slight reduction in the yield strength to 3428 MPa, the hardness reached a peak value of 936 HV. The presented results were obtained from the specimen fabricated by spark plasma sintering of mechanically alloyed powder.

Quantitative analysis of the strengthening mechanism in an HEA is rather complex because of insufficient information regarding the values of certain constant parameters. Using values estimated through the rule of mixtures can render theoretical calculations dubious, and even irrelevant, to the actual mechanism. Therefore, the mechanical behavior is examined in qualitative perspective. The main mechanisms underlying

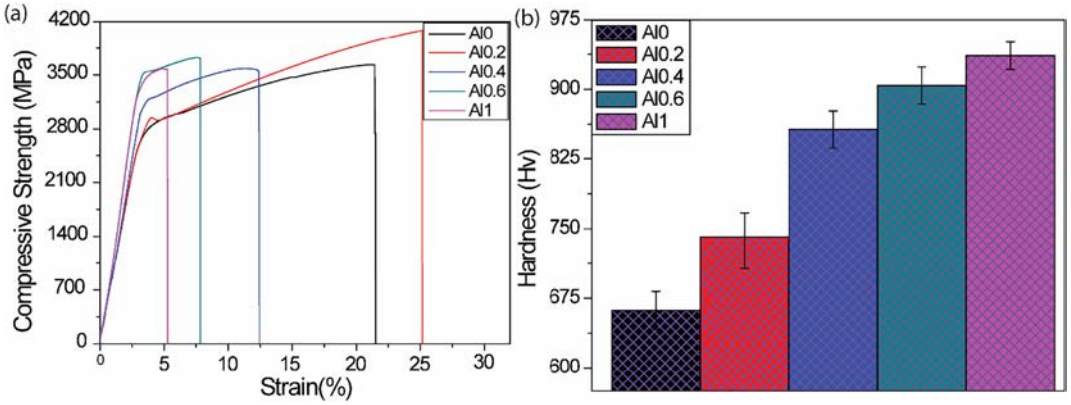

Fig. 7. Mechanical properties of the fabricated alloys. (a) Compressive strength and (b) Vickers hardness.

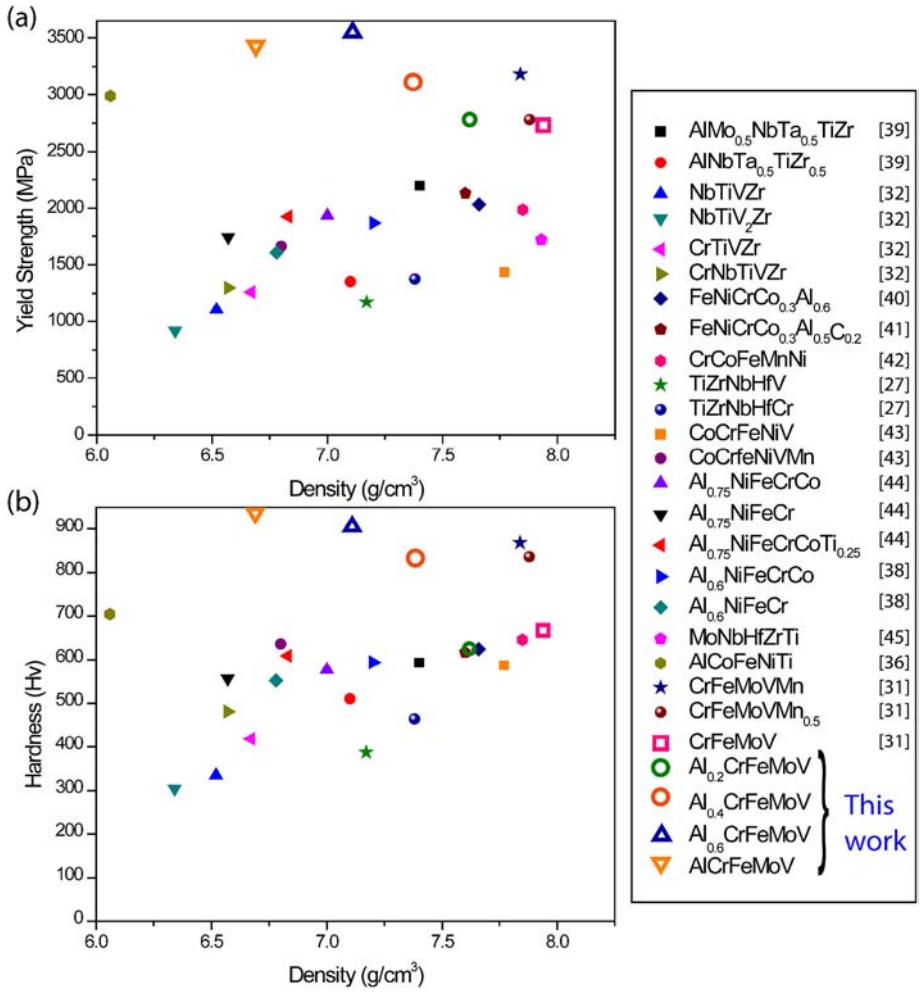

Fig. 8. (a) Compressive yield strength and (b) hardness as a function of density for the current alloys and previously reported high-entropy alloys (HEAs). The comparative data were extracted from [27,31,32,36,38,40–46].

the enhancement of compressive strength from 2730 MPa in Al-0 to 3552 MPa in Al-0.6 are solid solution strengthening and dispersion strengthening. The contribution of dispersion strengthening by Al/O inclusions can be calculated by using the Orowan equation due to non-coherent nature of the particles [5]. The calculated values from dispersion strengthening in Al-0, and Al-1 systems were 222 MPa, and 273 MPa respectively. The enhancement in strength by dispersion strengthening is not significant. Furthermore, the addition of Al might have played a role in improvement of solid solution strengthening due to large atomic size difference. If Fe and Cr with atomic sizes of 124 and 125 pm, respectively, are considered as solvents in an alloy, and V, Mo and Al with atomic sizes of 132, 136 and 143 pm, respectively, as solutes, then Al has the highest atomic size difference of 14%. This high atomic size difference significantly enhanced the strength of Al-containing alloys compared with the Al-0 system. The contribution of BCC1 and BCC2 phase to the strengthening was still mixed even after subtracting the contribution of dispersed Al/O phase due to ultrafine distribution of both phases. Therefore, it is hard to say how the BCC2 phase individually contributing to the strengthening of the systems.

The addition of Al dually influenced the properties of the CrFeMoV alloy by improving its strength (through solid solution and dispersion strengthening, and reducing the density of the system). The specific yield strengths of Al-0, Al-0.2, Al-0.4, Al-0.6 and Al-1 were 344, 365, 432, 500 and 512 MPa·cm^3/g, respectively. The yield strength and hardness as a function of density were compared with data for previously reported HEAs (Fig. 8). The results highlight the extraordinary mechanical properties of our quinary systems compared with any other previously reported HEA system having moderate density. The strength and hardness tend to increase with a reduction of density due to a higher concentration of Al. These exceptional mechanical features suggest a promising future for this alloy in many structural applications.

4. Conclusion

The variation in microstructural and mechanical properties of CrFeMoV HEA, which is an SSS, with the addition of Al was investigated. The Al$_x$CrFeMoV system was fabricated using powder metallurgy techniques by milling for the optimized time of 7 h, with methanol as a PCA. The addition of Al instigated the formation of a secondary phase (BCC2) enriched with V, and additionally Mo and Cr, in a BCC1 matrix. A thermodynamic analysis was in good agreement with the experimental results. The addition of Al greatly enhanced the mechanical properties and resulted in an exceptionally high specific yield strength of 512 MPa·cm^3·m^{-1} in Al^{-1}. The outstanding mechanical properties, which are better than those of any previously reported HEAs, low cost and low density of the current alloys hold great promise for a wide range of practical applications.

Acknowledgement

This research was supported by Basic Science Research Program through the National Research Foundation of Korea (NRF) funded by the Ministry of Science and ICT (NRF-2016R1E1A1A01943278); and National R&D Program through the National Research Foundation of Korea

(NRF) funded by the Ministry of Science and ICT (NRF-2015R1A5A1037627).

Author contribution

The main experimental work and manuscript writing was conducted by Ahmad Raza. The research was done under direct supervision of both Ho Jin Ryu and Soon Hyung Hong. Both of them also contributed in the revision and the improvement of the manuscript.

References

[1] D.J.M. King, S.C. Middleburgh, A.G. McGregor, M.B. Cortie, Predicting the formation and stability of single phase high-entropy alloys, Acta Mater. 104 (2016) 172–179.
[2] O.N. Senkov, D. Isheim, D.N. Seidman, A.L. Pilchak, Development of a refractory high entropy superalloy, Entropy 18 (3) (2016) 1–13.
[3] J.Y. He, et al., Effects of Al addition on structural evolution and tensile properties of the FeCoNiCrMn high-entropy alloy system, Acta Mater. 62 (1) (2014) 105–113.
[4] Y.F. Kao, T.D. Lee, S.K. Chen, Y.S. Chang, Electrochemical passive properties of AlxCoCrFeNi (x = 0, 0.25, 0.50, 1.00) alloys in sulfuric acids, Corros. Sci. 52 (3) (2010) 1026–1034.
[5] B. Kang, J. Lee, H. Jin, S. Hyung, Ultra-high strength WNbMoTaV high-entropy alloys with fi ne grain structure fabricated by powder metallurgical process, Mater. Sci. Eng. A 712 (December 2017) (2018) 616–624.
[6] L. Zhang, Y. Zhou, X. Jin, X. Du, B. Li, The microstructure and high-temperature properties of novel nano precipitation-hardened face centered cubic high-entropy superalloys, Scr. Mater. 146 (2018) 226–230.
[7] Z. Li, K.G. Pradeep, Y. Deng, D. Raabe, C.C. Tasan, Metastable high-entropy dual-phase alloys overcome the strength–ductility trade-off, Nature 534 (7606) (2016) 227.
[8] D.B. Miracle, O.N. Senkov, A critical review of high entropy alloys and related concepts, Acta Mater. 122 (2017) 448–511.
[9] J.W. Yeh, et al., Nanostructured high-entropy alloys with multiple principal elements: novel alloy design concepts and outcomes, Adv. Eng. Mater. 6 (5) (2004) 299–303+274.
[10] O.N. Senkov, J.D. Miller, D.B. Miracle, C. Woodward, Accelerated exploration of multi-principal element alloys for structural applications, Calphad Comput. Coupling Phase Diagr. Thermochem. 50 (2015) 32–48.
[11] A. Kumar, M. Gupta, An insight into evolution of light weight high entropy alloys: a review, Metals (Basel). 6 (9) (2016) 199.
[12] Z. Wang, Y. Huang, Y. Yang, J. Wang, C.T. Liu, Atomic-size effect and solid solubility of multicomponent alloys, Scr. Mater. 94 (2015) 28–31.
[13] X. Yang, Y. Zhang, Prediction of high-entropy stabilized solid-solution in multi-component alloys, Mater. Chem. Phys. 132 (2–3) (2012) 233–238.
[14] S. Guo, C.T. Liu, Phase stability in high entropy alloys: formation of solid-solution phase or amorphous phase, Prog. Nat. Sci. Mater. Int. 21 (6) (2011) 433–446.
[15] N. Yurchenko, N. Stepanov, G. Salishchev, Laves-phase formation criterion for high-entropy alloys, Mater. Sci. Technol. 33 (1) (2017) 17–22.
[16] M.G. Poletti, L. Battezzati, Electronic and thermodynamic criteria for the occurrence of high entropy alloys in metallic systems, Acta Mater. 75 (2014) 297–306.
[17] S. Guo, C. Ng, J. Lu, C.T. Liu, Effect of valence electron concentration on stability of fcc or bcc phase in high entropy alloys, J. Appl. Phys. 109 (10) (2011).
[18] F. Tian, L.K. Varga, N. Chen, J. Shen, L. Vitos, Ab initio design of elastically isotropic TiZrNbMoVx high-entropy alloys, J. Alloys Compd. 599 (2014) 19–25.
[19] Y.F. Ye, Q. Wang, J. Lu, C.T. Liu, Y. Yang, The generalized thermodynamic rule for phase selection in multicomponent alloys, Intermetallics 59 (2015) 75–80.
[20] Y.F. Ye, Q. Wang, J. Lu, C.T. Liu, Y. Yang, Design of high entropy alloys: a single-parameter thermodynamic rule, Scr. Mater. 104 (2015) 53–55.
[21] Y.F. Ye, Q. Wang, J. Lu, C.T. Liu, Y. Yang, High-entropy alloy: challenges and prospects, Mater. Today 19 (6) (2016) 349–362.
[22] X. Fu, C.A. Schuh, E.A. Olivetti, Materials selection considerations for high entropy alloys, Scr. Mater. 138 (2017) 145–150.
[23] F. He, et al., Strengthening the CoCrFeNiNb0.25 high entropy alloy by FCC precipitate, J. Alloys Compd. 667 (2016) 53–57.
[24] W.H. Liu, et al., Ductile CoCrFeNiMox high entropy alloys strengthened by hard intermetallic phases, Acta Mater. 116 (2016) 332–342.
[25] S.H. Joo, et al., Structure and properties of ultrafine-grained CoCrFeMnNi high-entropy alloys produced by mechanical alloying and spark plasma sintering, J. Alloys Compd. 698 (2017) 591–604.
[26] Y.D. Wu, et al., A refractory Hf25Nb25Ti25Zr25 high-entropy alloy with excellent structural stability and tensile properties, Mater. Lett. 130 (2014) 277–280.
[27] E. Fazakas, et al., Experimental and theoretical study of Ti20Zr20Hf 20Nb20X20 (X = v or Cr) refractory high-entropy alloys, Int. J. Refract. Met. Hard Mater. 47 (2014) 131–138.
[28] O.A. Waseem, H.J. Ryu, Powder metallurgy processing of a WxTaTiVCr high-entropy alloy and its derivative alloys for fusion material applications, Sci. Rep. 7 (1) (2017) 1–14.
[29] F. Otto, et al., Decomposition of the single-phase high-entropy alloy CrMnFeCoNi after prolonged anneals at intermediate temperatures, Acta Mater. 112 (2016) 40–52.
[30] O.N. Senkov, S.V. Senkova, C. Woodward, D.B. Miracle, Low-density, refractory multi-principal element alloys of the Cr-Nb-Ti-V-Zr system: microstructure and phase analysis, Acta Mater. 61 (5) (2013) 1545–1557.
[31] A. Raza, B. Kang, J. Lee, H.J. Ryu, S.H. Hong, Transition in microstructural and mechanical behavior by reduction of sigma-forming element content in a novel high entropy alloy, Mater. Des. 145 (2018) 11–19.
[32] O.N. Senkov, S.V. Senkova, D.B. Miracle, C. Woodward, Mechanical properties of low-density, refractory multi-principal element alloys of the Cr–Nb–Ti–V–Zr system, Mater. Sci. Eng. A 565 (2013) 51–62.
[33] O.N. Senkov, S.V. Senkova, C. Woodward, Effect of aluminum on the microstructure and properties of two refractory high-entropy alloys, Acta Mater. 68 (2014) 214–228.
[34] C.-J. Tong, et al., Microstructure characterization of Al x CoCrCuFeNi high-entropy alloy system with multiprincipal elements, Metall. Mater. Trans. A 36 (4) (2005) 881–893.
[35] R.S. Ganji, P. Sai Karthik, K. Bhanu Sankara Rao, K.V. Rajulapati, Strengthening mechanisms in equiatomic ultrafine grained AlCoCrCuFeNi high-entropy alloy studied by micro- and nanoindentation methods, Acta Mater. 125 (2017) 58–68.
[36] Z. Fu, et al., Microstructure and mechanical behavior of a novel Co20Ni20Fe20Al20Ti20 alloy fabricated by mechanical alloying and spark plasma sintering, Mater. Sci. Eng. A 644 (2015) 10–16.
[37] T.T. Shun, C.H. Hung, C.F. Lee, The effects of secondary elemental Mo or Ti addition in Al0.3CoCrFeNi high-entropy alloy on age hardening at 700 °C, J. Alloys Compd. 495 (1) (2010) 55–58.
[38] Z. Fu, W. Chen, H. Wen, Z. Chen, E.J. Lavernia, Effects of Co and sintering method on microstructure and mechanical behavior of a high-entropy Al 0.6 NiFeCrCo alloy prepared by powder metallurgy, J. Alloys Compd. 646 (2015) 175–182.
[39] Y. Zhang, Y.J. Zhou, J.P. Lin, G.L. Chen, P.K. Liaw, Solid-solution phase formation rules for multi-component alloys, Adv. Eng. Mater. 10 (6) (2008) 534–538.
[40] K.B. Zhang, et al., Microstructure and mechanical properties of CoCrFeNiTiAlxhigh-entropy alloys, Mater. Sci. Eng. A 508 (1–2) (2009) 214–219.
[41] J.M. Wu, S.J. Lin, J.W. Yeh, S.K. Chen, Y.S. Huang, H.C. Chen, Adhesive wear behavior of AlxCoCrCuFeNi high-entropy alloys as a function of aluminum content, Wear 261 (5–6) (2006) 513–519.
[42] W.R. Wang, W.L. Wang, J.W. Yeh, Phases, microstructure and mechanical properties of AlxCoCrFeNi high-entropy alloys at elevated temperatures, J. Alloys Compd. 589 (2014) 143–152.
[43] L.J. Santodonato, et al., Deviation from high-entropy configurations in the atomic distributions of a multi-principal-element alloy, Nat. Commun. 6 (2015) 5964.
[44] T. Yang, et al., Precipitation behavior of AlxCoCrFeNi high entropy alloys under ion irradiation, Sci. Rep. 6 (April) (2016) 32146.
[45] W. Chen, Z. Fu, S. Fang, H. Xiao, D. Zhu, Alloying behavior, microstructure and mechanical properties, J. Mater. 51 (2013) 854–860.
[46] G. Ghosh, M. Asta, First-principles calculation of structural energetics of Al-TM (TM = Ti, Zr, Hf) intermetallics, Acta Mater. 53 (11) (2005) 3225–3252.